Colloid and Polymer Science (2020) 298:549–558
https://doi.org/10.1007/s00396-020-04624-5

ORIGINAL CONTRIBUTION

Electrochemical formation of silver nanoparticles and their catalytic activity immobilised in a hydrogel matrix

Catherine M. Fox[1] · Tian Yu[1] · Carmel B. Breslin[1]

Received: 30 October 2019 / Revised: 10 January 2020 / Accepted: 20 February 2020 / Published online: 24 March 2020

Abstract

Silver nanoparticles were formed electrochemically in the presence of poly(*N*-vinylpyrrolidone) (PVP) to generate highly stable nanoparticles with a mean diameter of 12 nm. The optimised conditions involved formation at − 6.0 V vs Ag|Ag^+ with a PVP:Ag^+ ratio of 75:1. Particle agglomeration was observed when the PVP:Ag^+ ratio was reduced to 25:1 and when extended polarisation periods were employed. Using the optimised conditions, the silver nanoparticles remained stable for periods in excess of 2 months. The nanoparticles were immobilised inside a polyacrylamide hydrogel and used for the reduction of 4-nitrophenol. The rate constant obtained for the reduction of 4-nitrophenol was calculated as 7.1×10^{-4} to 1.6×10^{-3} s^{-1} depending on the amount of silver. The hydrogel–Ag composite was stable and could be stored for several months, while there was little change in the rate constant when it was repeatedly used.

Keywords Silver nanoparticles · Hydrogel · Electrochemical · Catalysis

Introduction

The formation and applications of metal nanoparticles have attracted considerable attention in recent years [1–10]. In particular, silver nanoparticles are widely studied and they have been employed in several areas, including food-related fields [1], with applications in reducing infectious diseases [2, 3], as sensors [4, 5] and in environmental science, mainly in water purification [6, 7]. Silver ions and silver nanoparticles have also been employed widely as antibacterial agents. It has been shown that silver nanoparticles are effective against a broad spectrum of bacteria, including both Gram-negative and Gram-positive bacteria [3]. In particular, they inhibit the growth of *Escherichia coli* [8] and MRSA [9]. The catalytic activity of silver nanoparticles is also well known [10–13]. The reduction of 4-nitrophenol to aminophenol with the addition of sodium borohydride is typically used as a model reaction. It is generally accepted that the borohydride transfers a hydrogen atom to the surface of the silver nanoparticle which, in turn, facilitates the reduction of the nitrophenol molecule. Generally, smaller silver nanoparticles, with narrow size distributions, show higher catalytic activity [14]. In addition to having a higher surface area to volume ratio, more efficient electron transfer occurs and higher rate constants are achieved. However, smaller silver nanoparticles are more susceptible to particle agglomeration and this results in a significant loss in the catalytic activity. Immobilisation of the particles onto or into a support material is one of the most effective measures in reducing particle agglomeration. Various materials have been employed successfully to immobilise silver nanoparticles [11–13]. Generally, the support material is immersed in a silver-containing solution and the incorporated silver ions are then reduced at/in the support [12, 13].

Silver nanoparticles and indeed other silver nanostructures, such as silver nanoplates, are easily synthesised and they are commonly formed using chemical reduction, where a reducing agent, such as sodium borohydride or sodium citrate, is employed to reduce Ag^+ to Ag^0 [15, 16]. This is followed by the formation of clusters which eventually leads to the generation of the silver nanoparticles. A protecting or capping reagent is also used to prevent particle agglomeration. While the chemical synthesis of silver nanoparticles is very successful and can be used to form well-defined nanoparticles with a narrow size distribution, the costs of the reagents, the release of hazardous by-products and the purification steps have prompted the development of more ‘greener’ approaches.

✉ Carmel B. Breslin
Carmel.Breslin@mu.ie

[1] Department of Chemistry, Maynooth University, Maynooth, Co. Kildare, Ireland

Consequently, biological methods have been developed, where fungi, bacteria and plant extracts are employed [17, 18]. These extracts contain reducing and/or capping reagents, with many plant extracts containing aldehydes and quinones. Other green processes include electrochemical methods and these can be used to generate large quantities of silver nanoparticles in relatively short periods of time. The most common approach is to employ sacrificial anodes, where the anode is dissolved to generate the metal cation, which is then combined with a stabiliser and reduced at the cathode to give stabilised colloidal particles [19, 20]. However, passivation of the anode can occur and the efficiency of the process may be reduced through the electrodeposition of the cations at the cathode in the cell. Furthermore, the solution usually only contains the protecting reagent, giving a low conductivity medium that requires high potentials to deliver the metal cations.

In this paper, silver nanoparticles were prepared in solution using electrochemical reduction, but with a silver salt dissolved in a supporting electrolyte to give a conducting solution. The electrochemical formation of silver nanoparticles is easily achieved as the Ag^+ ions are reduced on application of a potential below the standard reduction potential of the $Ag|Ag^+$ couple, making it possible to deposit silver nanoparticles and other silver nanostructures [21–23]. The reduction of Ag^+ in the presence of poly(*N*-vinylpyrrolidone), PVP, which is a well-known stabilising agent [21], was used to generate PVP-protected silver nanoparticles in solution, within a 5-min period, without the need for a reducing agent, or a sacrificial anode. Large negative overpotentials were employed to give rapid formation of the nanoparticles at room temperature. To the best of our knowledge, this approach, using a large negative constant potential in a silver-containing salt solution, has not been investigated and optimised for the formation of stable silver nanoparticles. The electrosynthesised particles were then immobilised within a polyacrylamide hydrogel and tested as a catalyst for the reduction of nitrophenol. Although the in situ synthesis of silver nanoparticles in hydrogels, where the hydrogel matrix is used as the reaction medium, is more commonly used to form hydrogel–nanoparticle composites, the electrochemically synthesised silver nanoparticles are easily dispersed within the hydrogel matrix and the silver nanoparticles facilitate the formation of the hydrogel.

Experimental and materials

Electrochemical formation of PVP-protected silver nanoparticles

PVP, $AgNO_3$ and KNO_3 were obtained from Sigma–Aldrich, while the platinum sheet electrodes (99.9%) were purchased from Goodfellow Metals. The platinum sheets were abraded using a Metaserve Universal polisher with water-lubricated silicon carbide paper to a 1200 grit grade, and they were then sonicated in an ethanol–water mixture and dried under a stream of air. The electrochemical reduction of Ag^+ was achieved using a Solartron (Model SI 1287) potentiostat in a typical three-electrode cell, with a $Ag|Ag^+$ pseudo-reference electrode, and two platinum sheet electrodes (1 × 5 cm length × width) as the working and counter electrodes. All experiments were carried out in deoxygenated solutions and the cell was covered to remove light. The applied potentials and concentrations of Ag^+ and PVP were varied to give stable silver nanoparticles with a narrow-size distribution. The optimised solution consisted of 50 mM $AgNO_3$ and 423.75 g dm^{-3} PVP to give a ratio of PVP:Ag^+ of 75:1, which was dissolved in a supporting 0.1 M KNO_3 electrolyte. The PVP content is expressed in g dm^{-3} as an exact molecular mass is not available (average molecular mass is 40,000 g mol^{-1}). The nanoparticles were generated under constant agitation at potentials ranging from − 0.10 to −6.0 V vs $Ag|Ag^+$. The potential of the silver pseudo-reference electrode was measured before and after the experiments, and no significant potential drift was observed.

Formation of a hydrogel with PVP-protected nanoparticles

The PVP-protected silver nanoparticles were incorporated into a polyacrylamide (PAAm) hydrogel composite. All solutions were purged with nitrogen for 20 min before any of the solutions were combined and also purged during formation of the gel. The acrylamide (4.0 g) monomer and *N*,*N*′-methylene-bis-acrylamide (MBA) (0.175 g) were dissolved in 10 mL of water. The PVP-protected silver nanoparticles dispersed in 10 mL of water were added to the monomer solution with stirring. Freshly made 1% ammonium persulfate (AP) solution and tetramethylethylenediamine (TEMED) were added with vigorous mechanical stirring to initiate polymerisation. The gels were then transferred to a glass vial (5 cm × 1 cm in diameter) and allowed to set at room temperature to give the hydrogel–Ag composites. After a 2-h period, the bottom of the glass tube was removed using a grinding wheel and the hydrogel cylinder was removed and cut into 3-mm discs using a sharp blade. Based on the amount of silver salt initially used, the mass of silver was estimated as 0.2 mg in each disc. The discs were suspended in deoxygenated deionised water and in the dark for 24 h to extract any unreacted reagents from the hydrogel.

Scanning electron microscopy (SEM) was performed on a Hitachi SEM model S-3200N instrument. The nanoparticles were dispersed onto a metal substrate, and Image J software was used to estimate the size of the particles. TEM measurements were carried out using a FEI Titan TEM. UV-visible spectroscopy was used to monitor the stability of the silver

nanoparticles. The solution collected from the electrochemical synthesis was diluted in some cases before the UV-Vis data were collected to give absorbance values lower than about 1.0. This dilution factor, if applied, is indicated in the figure captions. All measurements were performed using a Cary UV-visible spectrometer.

Reduction of 4-nitrophenol

Solutions of 4-nitrophenol and $NaBH_4$ were freshly made and purged with N_2 for 20 min. Three hydrogel discs were used and added to the combined solutions, 3 mL of 1.2×10^{-4} M 4-nitrophenol with 6 mL of 0.1 M $NaBH_4$ and stirred. The rate of the reduction reaction was monitored using UV-visible spectroscopy. Using this approach, the ratio of $NaBH_4$ to 4-nitrophenol was maintained at 1667:1. All experiments were repeated at least three times and the average values are shown with error bars.

Results and discussion

Formation of PVP-protected Ag nanoparticles

The silver nanoparticles were formed electrochemically using PVP which is a well-known protecting agent that can be employed to minimise agglomeration [21]. Initially, the influence of PVP on the electrochemical reduction of Ag^+ at a platinum substrate was studied and typical data are presented in Fig. 1. The data presented in Fig. 1a correspond to the first cycle while the steady-state voltammograms, recorded after 10 cycles, are presented in Fig. 1b. In the absence of PVP, the reduction of Ag^+ to Ag^0 is seen at about − 0.10 V vs $Ag|Ag^+$, while the reverse oxidation reaction occurs at approximately 0.10 V vs $Ag|Ag^+$. The addition of increasing amounts of PVP has little influence on the initial reduction of Ag^+ at the clean unmodified platinum substrate and the subsequent oxidation waves are only slightly reduced in the presence of PVP. However, as shown in Fig. 1b, the subsequent cycles are very different and the influence of PVP is clearly evident. In the PVP-containing solution, some of the silver ions will be free and some will be bound by PVP to give PVP–Ag^+. As the PVP–Ag^+ is large and bulky, it will diffuse more slowly to the electrode–solution interface. This is consistent with the shift in the reduction wave to more negative potentials (Fig. 1b). Reduction of the free Ag^+ occurs at a peak potential of − 0.10 V vs $Ag|Ag^+$, but the protected PVP–Ag^+ is reduced at − 0.14 V vs $Ag|Ag^+$. This 35- to 40-mV shift in the reduction potential is evident for all PVP concentrations, where the ratio of PVP:Ag^+ varies from 27:1 to 75:1 and this suggests that some additional process that is less dependent on the PVP:Ag^+ ratio may also occur. Gasparotto et al. [24] have shown that PVP adsorbs onto platinum in acidic solutions, inhibiting the characteristic hydrogen adsorption process. It appears that the added PVP also adsorbs onto the platinum substrate in this nitrate solution and the reduction of free Ag^+ and PVP–Ag^+ now proceeds at the PVP-modified surface to give a lower reduction potential. In the absence of PVP, the Ag^+ ions are reduced initially to form a layer, and then this silver layer serves as a surface for further nucleation, giving a broad reduction wave and the growth of silver deposits. Interestingly, the reduction peak is sharper in the PVP-containing solutions and this may be due to the ability of the adsorbed PVP to bind Ag^+ at the surface, facilitating more efficient electron transfer and the formation of protected Ag^0 that is not available as a surface for the further reduction of Ag^+.

Oxidation of the deposited Ag^0 appears as two overlapping oxidation waves, at 0.10 V and 0.16 V vs $Ag|Ag^+$, and there is a marked decrease in the magnitude of the oxidation wave in the presence of PVP. This clearly shows that two forms of silver are deposited. A decrease in the current for the peak at about 0.10 V vs $Ag|Ag^+$ shows that the amount of free Ag^0 is lowered with the addition of PVP, while the new peak that emerges at 0.15 V vs $Ag|Ag^+$ is consistent with the oxidation of PVP–Ag^0, which is more difficult to oxidise. The viscosity of the solution also appears to influence the amount of silver deposited. Higher ratios of PVP to Ag^+ give higher oxidation peak currents and this suggests that in the more viscous solutions, the electrochemically formed PVP–Ag^0 remains at the

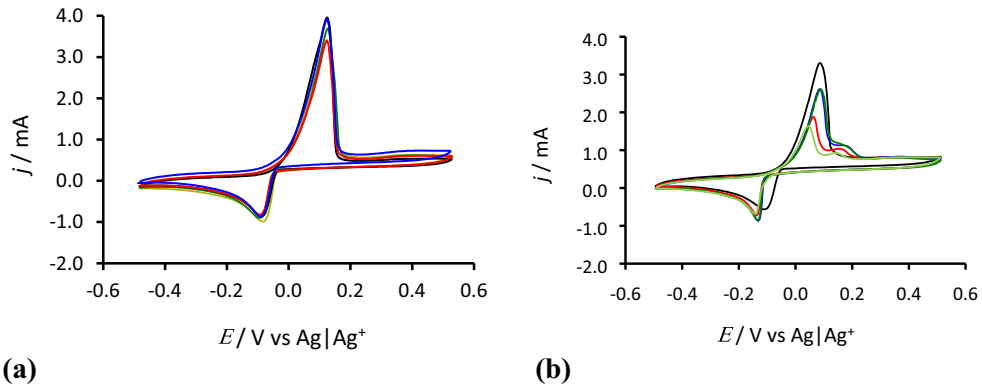

Fig. 1 Cyclic voltammograms recorded at 20 mV s^{-1} in 5 mM $AgNO_3$ and 0.1 M $NaNO_3$ with —, no PVP; —, 15 g dm^{-3} PVP; —, 20 g dm^{-3} PVP; —, 30 g dm^{-3} PVP; and —, 40 g dm^{-3} PVP (**a**) 1st cycle and (**b**) 10th cycle

surface and is available for oxidation, giving higher peak currents, while it diffuses into the bulk solution in the less viscous lower PVP concentrations.

As shown in Fig. 1, the reduction of Ag^+ is achieved at potentials lower than − 0.10 V vs $Ag|Ag^+$ and to facilitate the removal of the electrogenerated PVP–Ag^0 from the surface the solutions were continuously agitated. Current–time transients recorded in 50 mM $AgNO_3$ with 113 g dm^{-3} PVP are presented in Fig. 2, where the data are shown at fixed potentials of − 1.70 V and − 0.50 V vs $Ag|Ag^+$. The observed reduction currents are consistent with the conversion of Ag^+ to Ag^0 and these reach a near-steady state after about 10 s at − 1.70 V $Ag|Ag^+$ and 150 s at − 0.50 V vs $Ag|Ag^+$. While silver nanoparticles were formed at − 0.50 V vs $Ag|Ag^+$, a stream of a yellow-coloured solution became clearly visible at − 1.70 V $Ag|Ag^+$, indicating the formation of high concentrations of protected silver nanoparticles, within a short period of 200 s. The applied potential has a significant effect on the rate of formation of the nanoparticles, with higher steady-state currents observed at lower applied potentials. This is clearly evident in Table 1, where the steady-state currents are shown as a function of the applied potential. At potentials in the vicinity of − 1.70 V $Ag|Ag^+$ and lower, the reduction of H^+ and water occurs at the platinum surface and the high currents observed at these low potentials will contain contributions from Eqs. 1 and 2.

$$2H^+ + 2e^- \rightarrow H_2(g) \quad (1)$$

$$2H_2O + 2e^- \rightarrow H_2 + 2OH^- \quad (2)$$

The UV-Vis spectra of the PVP-protected silver nanoparticles formed at − 6.0 V vs $Ag|Ag^+$ are shown in Fig. 3 where the influence of the concentrations of PVP and $AgNO_3$, the electrodeposition period and reproducibility are summarised. As evident from Fig. 3a, a PVP:Ag^+ ratio of 75:1 gives the highest absorbance. A further increase of the PVP concentration to give a ratio of 100:1 gives a slightly lower absorbance and this appears to be related to a lower diffusion rate of the PVP–Ag^+ to the electrode surface in the more viscous medium. Variations in the PVP:Ag^+ ratio between 50:1 and 100:1 had little influence on the size and size distribution of the particles. A typical TEM micrograph, presented in the inset, shows the silver nanoparticles with an average size of about 12 nm in diameter. In Fig. 3b, a lower absorbance and broadening of the absorbance band is seen when the ratio of PVP:Ag^+ is reduced to 25:1, indicating particle agglomeration as insufficient PVP is available to protect the newly formed nanoparticles. The electrodeposition period has a significant influence (Fig. 3c). More nanoparticles are generated at 1200 s, but with increasing electrodeposition times, the decreasing absorbance coupled with band broadening indicates particle agglomeration, while at 6000 s, nearly complete agglomeration is seen, giving large silver deposits. The TEM micrograph, shown in the inset, was recorded after 2400 s and shows evidence of larger particle sizes and particle agglomeration. These results are consistent with electrochemical Ostwald ripening [25] and the theory of suspended electrodes, where the suspended nanoparticles become charged due to collisions with the electrode, facilitating further silver ion deposition to create larger particles [26]. It appears that while longer polarisation periods give rise to larger particle sizes, particle agglomeration becomes more difficult to avoid, due to Ostwald ripening, and therefore this approach is more suited to lower time periods. These data clearly show that the formation of the silver nanoparticles is very dependent on the experimental conditions. However, when the experimental conditions were optimised to give a PVP:Ag^+ ratio of 75:1, with deposition at − 6.0 V vs $Ag|Ag^+$ for about 600 s, giving a total fixed charge of 180 C, very good reproducibility was achieved, as illustrated in Fig. 3d. Identical λmax values of 405 nm with narrow bandwidths and very similar absorbance values were achieved with repeated experiments. The size and size distribution of the silver nanoparticles were estimated using TEM and SEM. A typical SEM micrograph is shown in Fig. 4a, where the average particle size was estimated at 12 nm, with the majority of particles between 9 and 14 nm (Fig. 4b), in good agreement with the TEM micrographs shown in Fig. 3.

Table 1 Steady-state current as a function of the applied potential in 50 mM $AgNO_3$, 0.1 M KNO_3 and 113 g dm^{-3} PVP

E/V vs $Ag|Ag^+$	*J*/mA
− 0.1	20.0 ± 1.6
− 0.3	30.1 ± 2.2
− 0.5	32.2 ± 2.0
− 0.8	35.3 ± 1.3
− 1.3	90.0 ± 4.0
− 2.0	180.8 ± 7.6
− 6.0	310.4 ± 6.6

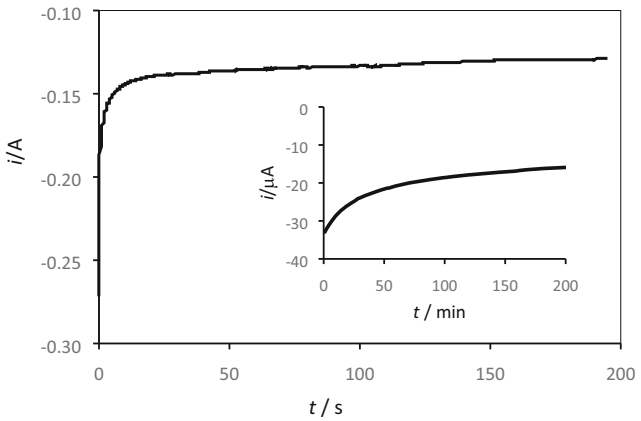

Fig. 2 Current transients recorded at Pt in 50 mM $AgNO_3$, 0.1 M KNO_3 and 113 g dm^{-3} PVP at − 1.7 V vs $Ag|Ag^+$ and at − 0.5 V vs $Ag|Ag^+$ (inset)

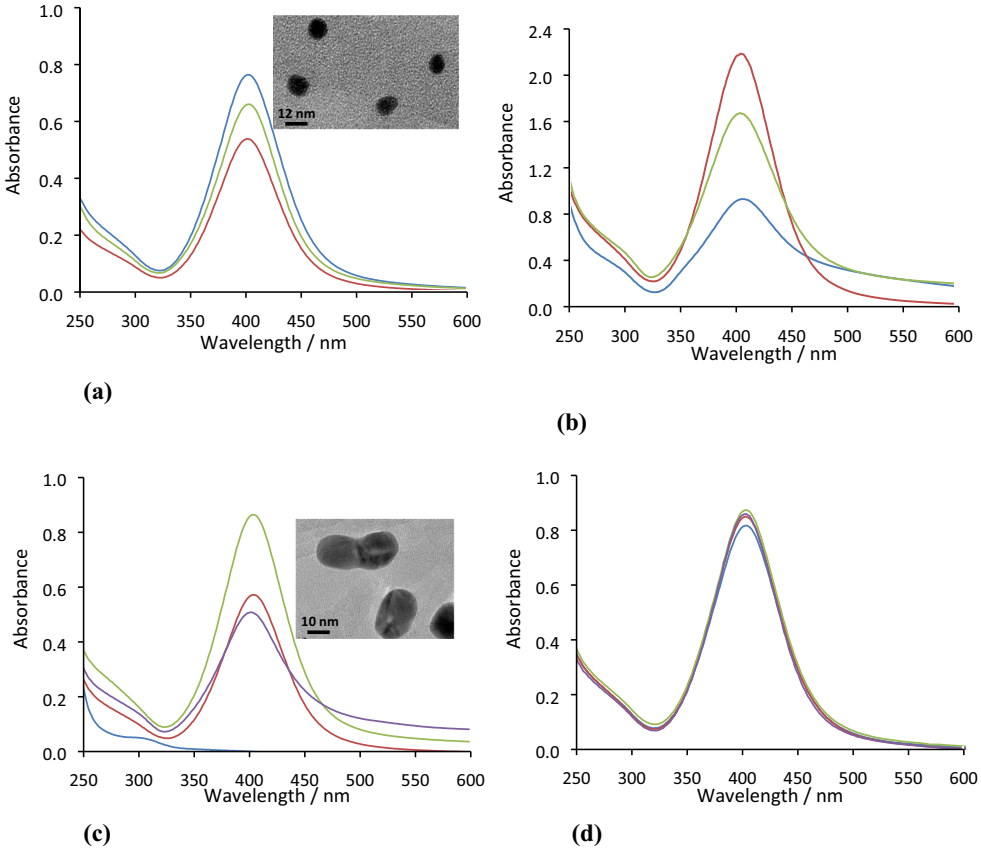

Fig. 3 UV-Vis absorption of a solution of silver nanoparticles (diluted by a factor of 120) generated at − 6.0 V vs $Ag|Ag^+$ for 600 s in 0.1 M KNO_3 (**a**) 5 mM $AgNO_3$ with —, 423.75 g dm^{-3} (75:1); —, 282.5 g dm^{-3} (50:1); and —, 565 g dm^{-3} PVP (100:1) with TEM in inset (**b**) 282.5 g dm^{-3} PVP with —, 5 mM; —, 50 mM; and —, 100 mM $AgNO_3$ (**c**) 50 mM $AgNO_3$ and 282.5 g dm^{-3} PVP for —, 600; —, 1200; —, 2400; and —, 6000 s with TEM micrograph recorded at 2400 s in inset and (**d**) five repeated experiments with 50 mM $AgNO_3$, 423.75 g dm^{-3} PVP (75:1) formed at − 6.0 V vs Ag/Ag^+ until a total charge of 180 C was passed

The stability of the nanoparticles was monitored over a 2-month period and these data are summarised in Fig. 5a. Very good stability is observed, with only a slight shift in the λmax and a small reduction in the absorbance. However, when aliquots of 5 mM $AgNO_3$ or 5 mM KNO_3 were added, or the solution was heated to 60 °C, instability was observed as shown in Fig. 5b where the maximum absorbance is plotted as a function of time. It is evident from Fig. 5b that very similar data are obtained with the addition of $AgNO_3$ and KNO_3, with a decrease in the absorbance after about 1 day, suggesting that the instability is due to the added nitrate or a change in the ionic strength and not due to the presence of additional Ag^+ ions. Although PVP is a large and steric nanoparticle protector compared with the more common electrostatic protectors, the protected nanoparticle can nevertheless be influenced by ionic strength. It has been shown that while citrate-protected particles are more susceptible to aggregation at high ionic strength, PVP-protected particles do suffer from some aggregation at high ionic strength [27]. Furthermore, the nitrate anion is an oxidant and it may behave like peroxides that have been shown to degrade PVP [28]. To test the possibility of PVP degradation in these media, the solution was

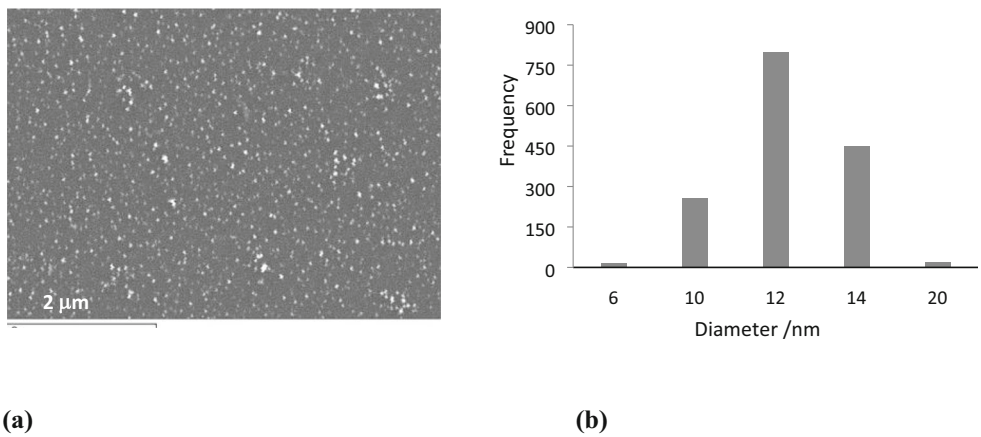

Fig. 4 (**a**) SEM micrograph of the silver nanoparticles and (**b**) size distribution

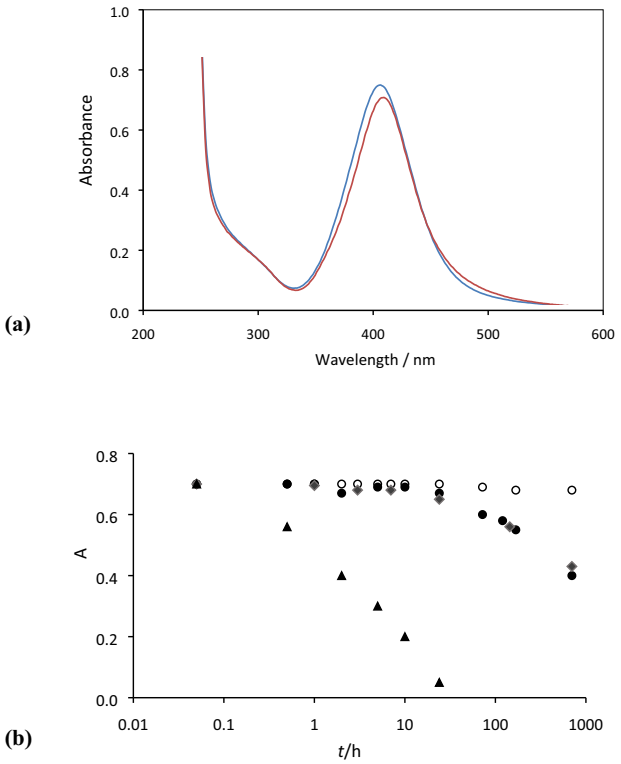

Fig. 5 (**a**) UV-Vis spectra of solutions of PVP-protected silver nanoparticles generated at − 6.0 V vs Ag/Ag^+ —, initially and —, after 2 months (solution diluted by a factor of 120) (**b**) absorbance at λ_{max} plotted as a function of time with ○, no additions; ●, 5 mM $AgNO_3$; ♦, 5 mM KNO_3; and ▲, heated at 60 °C

heated at 60 °C. This heating step resulted in a rapid decrease in the absorbance, as shown in Fig. 5b, with the formation of large silver deposits, and an increase in the absorbance between 250 and 350 nm, consistent with the formation of PVP oxidation and degradation products. These results show that while the electrochemically formed silver nanoparticles are stable for long periods, the addition of an oxidant, alterations in the ionic strength, or changes in the solution temperature reduce the protecting properties of PVP.

Reduction of nitrophenol at the hydrogel–Ag composite

The PVP-protected silver nanoparticles were incorporated within a polyacrylamide hydrogel and then used for the reduction of nitrophenol. The gelation times for the preparation of the hydrogel were about 15 to 20 min, using 400 μL of AP and 10 μL TEMED; however in the presence of the silver nanoparticles, instantaneous gelation was observed. The volumes of AP and TEMED were reduced to 300 μL and 5 μL, respectively, to control the gelation period. Similar effects have been observed with a silver electrode [29] and Ag^+ [30] and this has been attributed to the generation of radicals at a much faster rate from persulfate at the surface of silver. Given that the radicals are generated at the surface of the silver nanoparticles, this suggests that the silver nanoparticles are immobilised effectively within the forming hydrogel matrix. While these conditions are likely to partially degrade the PVP, the encapsulation of the nanoparticles within the forming hydrogel will serve to stabilise the nanoparticles.

The silver nanoparticle-containing hydrogels were then employed as a heterogeneous catalyst in the reduction of 4-nitrophenol using borohydride ions. This reduction reaction was chosen as a model as it is well known that as the borohydride, $B(OH)_4^-$, is converted to BH_4^- [31] and in the presence of H_2O molecules, H atoms are transferred to the silver surface. These adsorbed H atoms facilitate the reduction of 4-nitrophenol to 4-aminophenol [32]. In Fig. 6, UV-Vis spectra recorded as a function of time are shown for the hydrogel discs without (but with PVP) and with the incorporated silver nanoparticles, in the presence of 4.0×10^{-5} M 4-nitrophenol and 6.7×10^{-2} M $NaBH_4$. It is evident from the data presented in Fig. 6a that there is no decay in the peak at 404 nm that is due to the 4-nitrophenolate ion, which is formed in the presence of the alkaline solution generated on addition of $NaBH_4$. This clearly shows that the hydrogel matrix does not facilitate the reduction of nitrophenol. However, when the silver nanoparticles are added to the hydrogel matrix to give the hydrogel–Ag composite, the conversion of 4-nitrophenol to 4-aminophenol occurs (Fig. 6b) with a reduction in the absorbance at 404 nm and the appearance of a new band at 300 nm, which can be attributed to the aminophenol.

As the borohydride is present in large excess, the reaction can be assumed to be a pseudo-first-order reaction. Hence, the apparent rate constant k_{app} is defined using a first-order decay where c_t is the concentration of 4-nitrophenol at time t, and k_1 is the rate constant normalised to the surface area, S, Eq. 3. This equation can be reduced to the expression provided in Eq. 4, where the absorbance, A, is related to c_t through the Beer–Lambert law. The corresponding first-order plots are shown in Fig. 7a, where the logarithm of the absorbance at 404 nm is plotted as a function of time with freshly prepared hydrogel–Ag discs and rehydrated discs (stored in the dry state for 1 week). The good linearity is consistent with the pseudo-first-order decay (Eqs. 3 and 4). The apparent rate constant, k_{app}, was calculated as 7.1×10^{-4} s^{-1}. Furthermore, there is no significant difference in the rate constants when the freshly and rehydrated hydrogel–Ag composites are compared, indicating that the dried hydrogel–Ag discs remain as effective catalysts for the reduction of 4-nitrophenol.

$$\frac{dc_t}{d_t} = k_{app}c_t = k_1 S c_t \tag{3}$$

$$\ln A_t = \ln A_o - k_{qppt} t \tag{4}$$

It is well known that the rate of the catalytic reaction is dependent on the amount and surface area of the catalyst. In

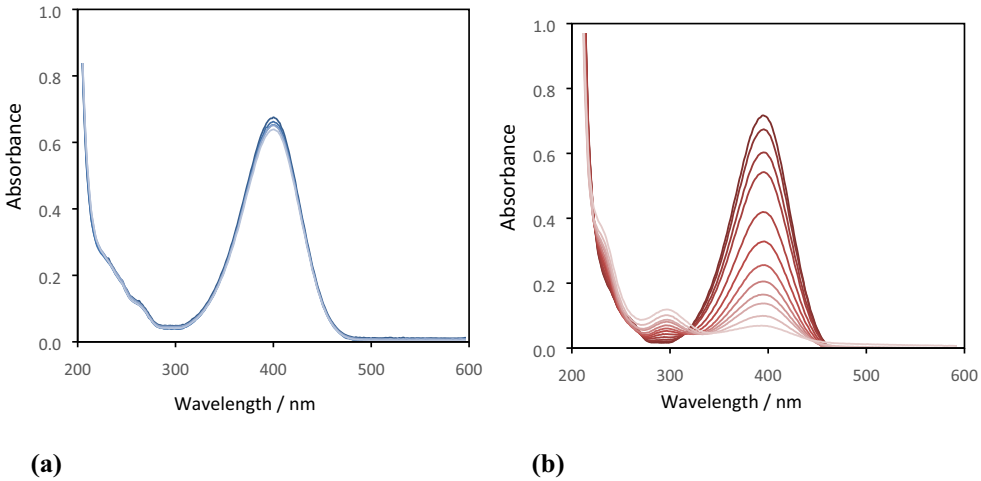

Fig. 6 UV-Vis spectra of 4.0×10^{-5} M 4-nitrophenol and 6.7×10^{-2} M $NaBH_4$ with (**a**) three hydrogel–PVP discs and (**b**) three hydrogel–Ag discs added

particular, as the reduction of nitrophenol involves adsorption processes, then the surface area of the silver nanoparticles incorporated within the hydrogel will have an influence on the rate constant. To illustrate this effect, the rate constant was determined as a function of the number of hydrogel beads used and the results of this study are presented in Fig. 7b. There is a near linear increase in the rate constant with an increasing number of discs, with a gradient of 2.3×10^{-4} s^{-1} per disc. This linear dependence is consistent with good dispersion of the silver nanoparticles within the hydrogel and good reproducibility in the silver loading from disc to disc.

The reusability of the hydrogel–Ag was further studied by repeated use in the reduction of nitrophenol. The hydrogel–Ag composite was used as a catalyst to reduce the nitrophenol solution for 60 min, and the hydrogel–Ag composite was then rinsed for 20 min in deionised water and then exposed to a fresh nitrophenol-containing solution. This was repeated several times and the results are summarised in Table 2. Overall, the reusability of the hydrogel–Ag catalyst is very good with only a slight reduction in the rate constant from 7.1×10^{-4} s^{-1} to 6.9×10^{-4} s^{-1} after four repeated uses, and from 7.1×10^{-4} s^{-1} to 6.7×10^{-4} s^{-1} after five repeated reduction experiments. While oxidation of the silver nanoparticles to Ag^+ ions and the leaching of these ions is a possible reaction for the hydrogel–Ag composite, the presence of the reducing agent, $NaBH_4$, is likely to inhibit this oxidation reaction and maintain the silver in the reduced Ag^0 state. Instead, this small decrease in the rate constant can be explained in terms of the slow diffusion of the 4-aminophenol from the hydrogel matrix, which potentially blocks the nitrophenol from the Ag nanoparticles. Indeed, it was found that the rate constant was returned to its initial value of 7.1×10^{-4} s^{-1} on rinsing the hydrogel–Ag discs in deionised water for 24 h, lending support to the slow diffusion of nitrophenol and aminophenol within the hydrogel–Ag composite. The slow diffusion within the hydrogel is further evident in Fig. 8 where cyclic voltammograms recorded at a platinum wire electrode and at the platinum wire encapsulated within the hydrogel–Ag matrix in a ferricyanide-containing electrolyte are compared. Oxidation of the ferrocyanide probe is clearly evident (Eq. 5) during the forward cycle, while reduction (Eq. 6) is evident during the reverse cycle at the exposed platinum wire, with a peak separation close to the ideal value of 0.057 V for a reversible reaction. However, when the platinum electrode is surrounded by the hydrogel–Ag composite, much lower peak currents are observed, consistent with poor diffusion of the ferricyanide probe within the hydrogel matrix. Furthermore, the peak separation is significantly higher than 0.057 V.

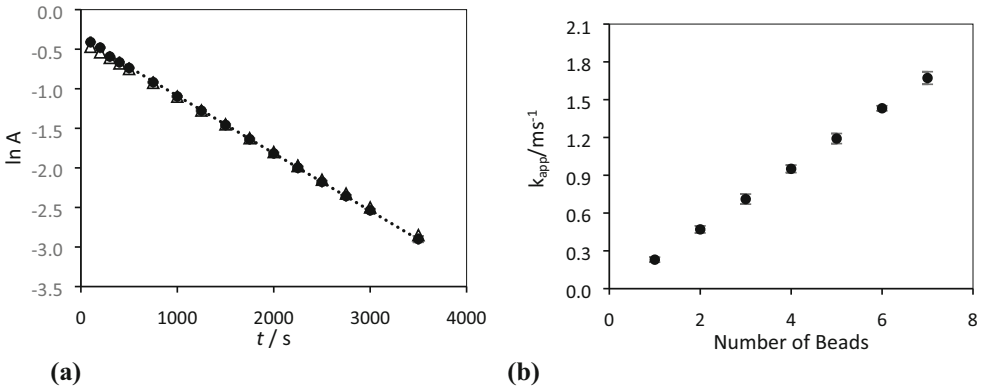

Fig. 7 (**a**) Logarithm of absorbance at λmax as a function of time for the catalytic reduction of 4-nitrophenol in 4.0×10^{-5} M 4-nitrophenol and 6.7×10^{-2} M $NaBH_4$ with freshly prepared discs ● and rehydrated discs Δ, (**b**) rate constant as a function of the number of hydrogel–Ag discs

Table 2 Reusability of the hydrogel–Ag composites in the reduction of 4-nitrophenol

k_{app}/s^{-1}	Number of times used
$(7.1 \pm 0.2) \times 10^{-4}$	1
$(7.0 \pm 0.3) \times 10^{-4}$	2
$(6.8 \pm 0.1) \times 10^{-4}$	3
$(6.9 \pm 0.2) \times 10^{-4}$	4
$(6.7 \pm 0.2) \times 10^{-4}$	5

$$Fe(CN)_6^{4-} \rightarrow Fe(CN)_6^{3-} + e^- \quad (5)$$

$$Fe(CN)_6^{3-} + e^- \rightarrow Fe(CN)_6^{4-} \quad (6)$$

It is difficult to compare directly the rate constants obtained to other literature reports, as in some cases theoretical specific surface areas are used [32], while in others the rate constant is normalised to the silver concentration used in the original synthesis of the particles [33]. In many cases, the silver nanoparticles are suspended free in solution and the rate constants are expressed in terms of the concentration in solution and the specific surface area [34]. Moreover, the rate is not only dependent on the surface area of the catalyst but also the rate of diffusion of reactants and products within the hydrogel matrix will have a clear influence on the conversion of nitrophenol to aminophenol. Nevertheless, this study compares well with data reported by Lu and co–workers, where apparent rate constants of 7.0×10^{-4} s^{-1} were reported for the reduction of nitrophenol using a poly(vinyl alcohol) matrix loaded with silver nanoparticles [35]. However, a higher value of 3.3×10^{-2} s^{-1} has been reported by Mao et al. [13] using silver nanoparticles dispersed on polyacrylamide/polypyrrole/graphene oxide sheets. Using the estimated mass of silver in each disc (0.2 mg), the normalised rate constant, k_{nor}, was calculated as 0.188 $mmol^{-1}$ s^{-1}, which compares well with values reported by Zhang et al. [33] of 0.134 and 0.148 $mmol^{-1}$ s^{-1}. While the rate constants obtained in this work are comparable with literature values, these hydrogel composites have good reusability and can be stored in the dehydrated state for several days without any loss in activity and they are also easily removed from the solution phase.

Leaching of the silver nanoparticles from the hydrogel matrix was monitored by immersing a single hydrogel disc in deionised water and then the solution was monitored at different time intervals using UV-visible spectroscopy. The resulting data are summarised in Fig. 9, where it is evident that there is very little leaching of the silver nanoparticles over a 24-h period. The absorbance only reaches a value of about 0.04 in a 10-mL volume. However, at longer immersion times, after 2 weeks, a more pronounced absorbance band centred at about 420 nm is evident and the absorbance increases further with the λmax shifting to a longer wavelength of 448 nm following an immersion period of 3 weeks. This increasing λmax indicates particle agglomeration, which becomes more evident when higher amounts of the silver nanoparticles are leached from the hydrogel. It appears that oxidation of the silver nanoparticles occurs as there is a sufficient concentration of dissolved oxygen in the water to corrode the silver nanoparticles. The leached Ag^+, or Ag^+ generated from the corrosion of the released particles, facilitates further particle agglomeration, giving rise to the increasing λmax. Indeed, it has been shown that Ag^+ ions are released from silver nanoparticles, with the extent of dissolution depending on the size of the particle and the pH of the solution. This dissolution process has been attributed to the oxidation of the particles by O_2 dissolved in solution and with the release of chemisorbed Ag^+ [36, 37], while a two-step process was more recently described, where the initial formation of silver oxides at the nanoparticles is followed by the dissolution of this oxide phase leading to the release of silver ions [38]. As the silver

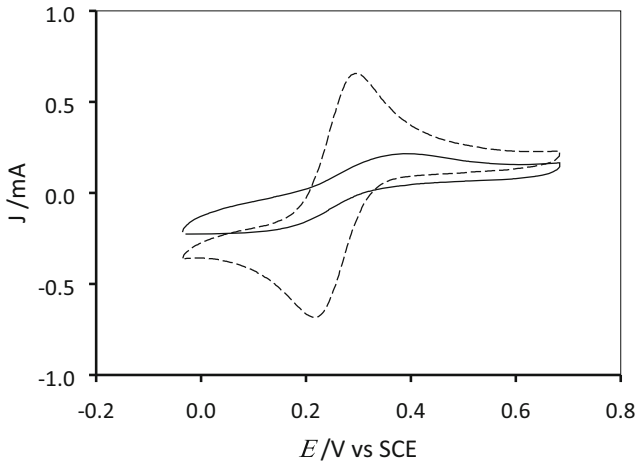

Fig. 8 Cyclic voltammograms recorded at 20 mV s^{-1} in 0.01 M $K_3Fe(CN)_6$ and 0.1 M Na_2SO_4 at ——, platinum surrounded by the hydrogel–Ag composite and – – –, pure platinum electrode

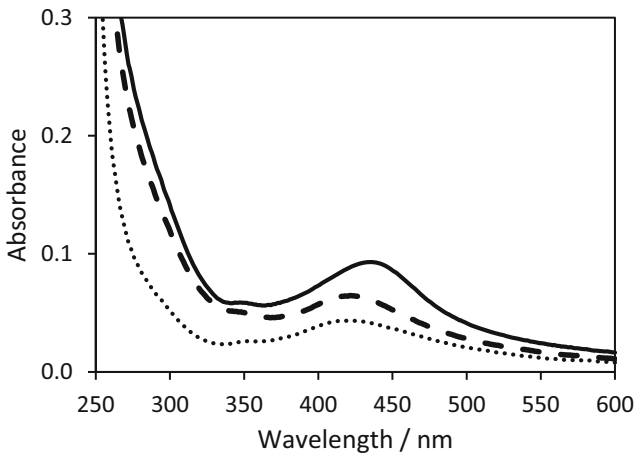

Fig. 9 Leaching of silver from hydrogel–Ag discs recorded after • • • •, 24 h; — —, 2 weeks; and ——, 3 weeks

nanoparticles are small, with an average diameter of approximately 12 nm, they are more prone to oxidation than larger nanoparticles [37] and this will facilitate the release of Ag^+. Although the release of silver nanoparticles from the hydrogel is possible due the large free volume and diffusion of water into and out of the hydrogel, the release of silver nanoparticles is slow, as evident in Fig. 9.

Conclusions

Highly stable silver nanoparticles with a narrow size distribution and with an average diameter of about 12 nm were formed in solution using an electrochemical approach, where the particles were formed rapidly at − 6.0 V in a silver-containing solution with PVP as a protecting agent. These nanoparticles were incorporated and immobilised within a polyacrylamide hydrogel. The presence of the silver nanoparticles accelerated the rate of formation of the gel, suggesting that the nanoparticles are wrapped within the forming gel. The hydrogel–Ag composite showed good catalytic activity for the reduction of 4-nitrophenol in the presence of $NaBH_4$, which also prevented the oxidation or corrosion of the silver nanoparticles, giving the hydrogel–Ag composite good stability and reusability. Although, hydrogels have a much larger free volume that other polymer systems and the release of the particles may be expected, it appears that the synthetic conditions, where the silver nanoparticles are involved in the reactions associated with the formation of the gel, give rise to the formation of well-bound silver nanoparticles that are slow to release.

Funding information This research work was funded by the Irish Research Council, Ireland.

Compliance with ethical standards

Conflict of interest The authors declare that they have no conflict of interest.

References

1. Sanpui P, Murugadoss A, Prasad PVD, Ghosh SS, Chattopadhyay A (2008) The antibacterial properties of a novel chitosan–Ag nanoparticle composite. Int J Food Microbiol 124:142–146
2. Zazo H, Colino CI, Lanao JM (2016) Current applications of nanoparticles in infectious diseases. J Control Release 224:86–102
3. Campoccia D, Montanaro L, Arciola CR (2013) A review of the biomaterials technologies for infection–resistant surfaces. Biomaterials 34:8533–8554
4. Branagan D, Breslin CB (2019) Electrochemical detection of glucose at physiological pH using gold nanoparticles deposited on carbon nanotubes. Sensors Actuators B Chem 282:490–499
5. Pedre I, Battaglini F, Delgado GJL, Sanchez –Loredo MG, Gonzalez GA (2015) Detection of thiourea from electrorefining baths using silver nanoparticles-based sensors. Sensors Actuators B Chem 211:515–522
6. Kim J–H, Van der Bruggen B (2010) The use of nanoparticles in polymeric and ceramic membrane structures: review of manufacturing procedures and performance improvement for water treatment. Environ Pollut 158:2335–2349
7. Khan ST, Malik A (2019) Engineered nanomaterials for water decontamination and purification: from lab to products. J Hazard Mater 363:295–308
8. Dror– Ehre A, Mamane H, Belenkova T, Markovich G, Adin A (2009) Silver nanoparticle–*E. coli* colloidal interaction in water and effect on *E. coli* survival. J Colloid Interface Sci 339:521–526
9. Surwade P, Ghildyal C, Weikel C, Luxton T, Peloquin D, Fan X, Shah V (2019) Augmented antibacterial activity of ampicillin with silver nanoparticles against methicillin–resistant *Staphylococcus aureus* (MRSA). J Antibiotics 72:50–53
10. Gangila A, Podila R, Karanam RML, Janardhana C, Rao AM (2011) Catalytic reduction of 4-nitrophenol using biogenic gold and silver nanoparticles derived from breynia rhamnoides. Langmuir 27:15268–15274
11. Zhu M, Wang C, Meng D, Diao G (2013) In situ synthesis of silver nanostructures on magnetic Fe_3O_4@C core–shell nanocomposites and their application in catalytic reduction reactions. J Mater Chem A 1:2118–2125
12. Mao H, Ji C, Liu M, Cao Z, Sun D, Xing Z, Chen X, Zhang Y, Song X–M (2018) Enhanced catalytic activity of Ag nanoparticles supported on polyacrylamide/polypyrrole/graphene oxide nanosheets for the reduction of 4–nitrophenol. Appl Surf Sci 434:522–533
13. Sahiner N, Karakoyun N, Alpaslan D, Aktas N (2013) Biochar–embedded soft hydrogel and their use in Ag nanoparticle preparation and reduction of 4–nitro phenol. Int J Polym Mater Polym Biomaterials 62:590–595
14. Fievet F, Ammar-Merah S, Brayner R, Chau F, Giraud M, Mammeri F, Peron J, Piquemal J-Y, Sicard L, Viau G (2018) The polyol process: a unique method for easy access to metal nanoparticles with tailored sizes, shapes and compositions. Chem Soc Rev 47:5187–5233
15. Zhang Q, Li N, Goebl J, Lu Z, Yin Y (2011) A systematic study of the synthesis of silver nanoplates: is citrate a "magic" reagent? J Am Chem Soc 133:18931–18939
16. Bastús NG, Merkoçi F, Piella J, Puntes V (2014) Synthesis of highly monodisperse citrate–stabilized silver nanoparticles of up to 200 nm: kinetic control and catalytic properties. Chem Mater 26:2836–2846
17. Mittal AK, Chisti Y, Banerjee UC (2013) Synthesis of metallic nanoparticles using plant extracts. Biotechnol Adv 31:346–356
18. Ahmed S, Ahmad M, Swami BL, Ikram S (2016) A review on plants extract mediated synthesis of silver nanoparticles for antimicrobial applications: a green expertise. J Adv Res 7:17–28
19. Kuntyi OI, Kytsya AR, Mertsalo IP, Mazur AS, Zozula GI, Bazylyak LI, Topchak RV (2019) Electrochemical synthesis of silver nanoparticles by reversible current in solutions of sodium polyacrylate. Colloid Polym Sci 297:689–695
20. Thuc DT, Huy TQ, Hoang LH, Tien BC, Chung PV, Thuy NT, Le A-T (2016) Green synthesis of colloidal silver nanoparticles through electrochemical method and their antibacterial activity. Mater Lett 181:173–177
21. Yin B, Ma H, Wang S, Chen S (2003) Electrochemical synthesis of silver nanoparticles under protection of poly(N–vinylpyrrolidone). J Phy Chem B 107:8898–8904
22. Zhao F, Zhou M, Wang L, Huang Z, Chu Y (2019) One–step voltammetric deposition of L–proline assisted silver nanoparticles modified glassy carbon electrode for electrochemical detection of hydrogen peroxide. J Electroanal Chem 833:205–212
23. Arvinte A, Crudu I–A, Doroftei F, Timpu D, Pinteala M (2018) Electrochemical codeposition of silver–gold nanoparticles on

CNT–based electrode and their performance in electrocatalysis of dopamine. J Electroanal Chem 829:184–193
24. Gasparotto LHS, Gomes JF, Tremiliosi– Filho G (2011) Cyclic–voltammetry characteristics of poly(vinyl pyrrolidone) (PVP) on single–crystal Pt surfaces in aqueous H_2SO_4. J Electroanal Chem 663:48–51
25. Redmond PL, Hallock AJ, Brus LE (2005) Electrochemical Ostwald ripening of colloidal Ag particles on conductive substrates. Nano Lett 5:131–135
26. Socol Y, Abramson O, Gedanken A, Meshorer Y, Berenstein L, Zaban A (2002) Suspensive electrode formation in pulsed sonoelectrochemical synthesis of silver nanoparticles. Langmuir 18:4736–4740
27. Zhang H, Zhang C (2014) Transport of silver nanoparticles capped with different stabilizers in water saturated porous media. J Mater Environ Sci 5:231–236
28. Suave J, José HJ, Moreira RFPM (2018) Photocatalytic degradation of polyvinylpyrrolidone in aqueous solution using TiO_2 /H_2O_2 /UV system. Environ Technol 39:1404–1412
29. Yildiz G, Çatalgil– Giz H, Kadirgan F (2000) Electrochemically prepared acrylamide/N,N′-methylene bisacrylamide gels. J Appl Electrochem 30:71–75
30. Singh A (2011) Synthesis and applications of polyacrylamide gels catalyzed by silver nitrate. J Appl Polym Sci 119:1084–1089
31. Guella G, Zanchetta C, Patton B, Miotello A (2006) New insights on the mechanism of palladium–catalyzed hydrolysis of sodium borohydride from 11B NMR measurements. J Phys Chem B 110: 17024–17033
32. Wunder S, Polzer F, Lu Y, Mei Y, Ballauff M (2010) Kinetic analysis of catalytic reduction of 4–nitrophenol by metallic nanoparticles immobilized in spherical polyelectrolyte brushes. J Phys Chem C 114:8814–8820
33. Zhang W, Tan T, Wang W, Qiu X, Qiao X, Chen J (2012) Facile template-free synthesis of silver nanodendrites with high catalytic activity for the reduction of p-nitrophenol, J. Hazard Mater 217-218:36–42
34. Silvestri D, Waclawek S, Venkateshaiah A, Krawczyk K, Sobel B, Padil VVT, Cernik M, Varma RS (2020) Synthesis of Ag nanoparticles by a chitosan-poly(3-hydroxybutyrate) polymer conjugate and their superb catalytic activity. Carbohydrate Polym 232:115806
35. Lu Y, Spyra P, Mei Y, Ballauff M, Pich A (2007) Composite hydrogels: robust carriers for catalytic nanoparticles. Macromol Chem Phys 208:254–261
36. Dobias J, Bernier– Latmani R (2013) Silver release from silver nanoparticles in natural water systems. Environ Sci Technol 47: 4140–4146
37. Peretyazhko TS, Zhang Q, Colvin VL (2014) Size–controlled dissolution of silver nanoparticles at neutral and acidic pH conditions: kinetics and size changes. Environ Sci Technol 48:11954–11961
38. Adamczyk Z, Ocwieja M, Mrowiec H, Walas S, Lupa D (2016) Oxidative dissolution of silver nanoparticles: a new theoretical approach. J Colloid Interface Sci 469:355–364